

STRESS INTENSITY FACTORS FROM STRESS ANALYSIS OF AN EQUIVALENT HOLE

Paolo Livieri

*Department of Engineering, University of Ferrara,
via Saragat 1, 44122 Ferrara, Italy, paolo.livieri@unife.it*

Abstract

In this paper, on the basis of the stress analysis of an equivalent model, the stress intensity factors (SIF) of a crack have been evaluated. In the stress analysis, the crack is substituted by an equivalent hole equal in size to the length of the crack. The method is based on the evaluation of the hoop stress on the free border of the equivalent hole and the subsequent calculation of the J-integral ($J_{V\rho}$) as a parameter related to the SIF. Alternatively, if the hoop stress on the free border cannot be evaluated, the stress analysis can be performed on the surface in the neighbourhood of the hole.

In order to validate the method, two experimental cases have been considered: a plate with two different bore diameters of 50% and 20% of the plate width, respectively. The stress analysis was performed by means of strain gauges attached to the free border. For the plate with the smaller bore, the strain gauges were also attached to the surface near the hole. In this way, the strain approach can be extended to thin plates or when it is not possible to attach the strain gauges to the free border of the hole.

Key words: stress intensity factor, strain gauge, stress analysis, J-integral

1. INTRODUCTION

The measurement of some physical quantities related to the displacement field or to the strain field in the neighbourhood of the crack tip allows the researcher to calculate the stress intensity factor (SIF). The direct evaluation of SIF from experimental analysis requires the use of optical techniques [1, 2] or accurate measurements of the temperature variation [3]. Due to the small size of the area where the high stress gradient occurs, the measurements must be very localised and, if possible, also be very accurate. The use of a common strain gauge with traditional grids (length of some millimetres), is not normally able to capture the local effect due to a singular stress field. On the other hand, the use of a strain gauge gives an engineer and a reliable response of stress measurements [4]. The application of a strain gauge with traditional grids is used, for example, in the field of welded joint integrity for the evaluation of structural stress [5,6,7]. The local stress field needed for fatigue assessments is extrapolated by means of the experimental strain measurements made in two or three points near the weld toe. However, the extrapolation at the weld toe is a difficult task because the trend of stress is the sum of the singular symmetric and skew-symmetric stress field related to Williams eigenvalue [8, 9] and many choices are possible [6,7].

As far as the SIF assessments are concerned, in order to avoid an analysis of a singular stress field, the crack could be replaced by an elliptical notch of the same size. This idea was proposed by Irwin in reference [10] and was supported by Neuber's results [11]. Under mode I loadings, Irwin verified that the product of peak stress σ_{\max} by the square root of the notch tip radius ρ gave the SIF when ρ converges to zero. Unfortunately, for a mode II loading, the stress at the notch tip is null and this gives some problems when assessing the mode II SIF (see for instance references [12, 13]). So that, the peak stress at the notch tip, as reported by Sih and Liebowitz [14], can be replaced by the maximum hoop stress due to the mode II loading. Alternatively, as shown in reference [15], the J-integral may be helpful to analyse the singularity of the stress field for cracks as introduced by Rice [16]. For elliptical, parabolic and hyperbolic notches as well as V-sharp notches, the use of the classical J-integral was generalised in Refs [17, 18]. In these cases, the J-integral is not strictly a path-independent integral [19]. To ensure clarity, the J-integral applied to a generic notch is indicated as $J_{V\rho}$, whereas the symbol J is used for the classical J-integral evaluated for a crack. In order to improve accuracy in the use of an ellipse as an equivalent notch, in Ref. [20] the component of J-integral related to the asymptotic

behaviour that tends to zero when the ellipse collapses in a crack, was neglected also for a finite value of the notch tip. The accuracy regarding the notch tip methods greatly increases up to the point that the crack could be replaced by a circle in engineering applications [20].

The aim of the paper is to give a simplified procedure for the evaluation of the stress intensity factors of cracks subjected to in-plane mixed mode loadings (mode I plus mode II). The procedure is performed to give an engineering response both for numerical or experimental investigations. The crack is substituted by an equivalent hole and the stress analysis is addressed on the hoop stress on the free border. The procedure is validated by means of strain gauge measurements by directly attaching the strain gauge to the free border of the bore, or to the surface of the plate near the border. The results obtained experimentally are compared with those given by analytical or numerical FE analysis.

2. Hoop Stress along the notch border of elliptical notches

The stress along the free border of an elliptical notch was obtained by Inglis in the classical solution reported in Ref. [21]. The ellipse was considered as an isolated notch under remote loading. Recently, by making use of the generalised plane strain hypothesis, an approximate stress field theory has been developed by Zappalorto and Lazzarin [22]. The generalised plane strain hypothesis reduces the notch problem into a common bi-harmonic equation governing the solution of the plane problem and into a harmonic equation governing the antiplane elasticity problem. They considered the case of a slim inclined elliptic hole in a finite thickness plate subjected to a remote tensile load.

When the ellipse cannot be considered an isolated notch or a stress assumes a particular configuration as in Figure 1, for a linear elastic material, the hoop stress along the free border of the ellipse can be evaluated with high accuracy by considering the solution proposed in Ref. [20].

With reference to Figure 1, the σ_θ hoop stress on the free border on an ellipse with semi-axis (a, b) is given by:

$$\sigma_\theta = \lambda_1 \sigma_{\theta,1} + \lambda_2 \sigma_{\theta,2} + \lambda_3 \sigma_{\theta,3} \quad (1)$$

where the λ_i are linear coefficients of combination that establish the final shape of the stress along the free border, and the dimensionless $\sigma_{\theta,i}$ stress functions result:

$$\sigma_{\theta,1} = \frac{e^{2\xi_0}}{1+2\frac{a}{b}} \left[\frac{\sinh 2\xi_0 (1+e^{-2\xi_0})}{\cosh 2\xi_0 - \cos 2\eta} - 1 \right] \quad (2)$$

$$\sigma_{\theta,2} = \frac{2ab e^{2\xi_0}}{(a+b)^2} \left[\frac{\sin 2\eta}{\cosh 2\xi_0 - \cos 2\eta} \right] \quad (3)$$

$$\sigma_{\theta,3} = \left[\frac{e^{2\xi_0} \cos 2\eta - \sinh 2\xi_0 - 1}{\cosh 2\xi_0 - \cos 2\eta} \right] \quad (4)$$

where $\xi_0 = \operatorname{arctanh} \frac{b}{a}$, $x = a \cdot \cos \eta$ and $y = b \cdot \sin \eta$ with $\eta \in [0, 2\pi]$.

The stresses $\sigma_{\theta,1}$ and $\sigma_{\theta,3}$ are symmetrical whereas $\sigma_{\theta,2}$ is a skew-symmetric function. The accuracy in stress approximation was discussed in [20] and the stress can be acceptably estimated with an average percent error ranging between 1 and 3%. The percent error $e_{\%}$ is defined in an interval $[\alpha_1, \alpha_2]$ with respect to the stress $\sigma_{\theta,FE}$ evaluated by means of finite element (FE) analysis:

$$e_{\%} = \frac{\int_{\alpha_1}^{\alpha_2} |\sigma_{\theta,Eq.1} - \sigma_{\theta,FE}| d\eta \cdot 100}{\int_{\alpha_1}^{\alpha_2} |\sigma_{\theta,FE}| d\eta} \quad (5)$$

In this work, we consider only the case of circular notches because a circular hole is easier to obtain than an elliptical one from an experimental point of view. So that, the dimensionless stress $\sigma_{\theta,i}$ (2-4) can be simplified as follows:

$$\sigma_{\theta,1} = \frac{1}{3} + \frac{2}{3} \cos 2\eta \quad (6)$$

$$\sigma_{\theta,2} = \sin 2\eta \quad (7)$$

$$\sigma_{\theta,3} = 2 \cos 2\eta - 1 \quad (8)$$

Figure 2 shows an example of stress approximation by means of stresses (6–8). The λ_i linear coefficients are calculated by imposing a minimum averaged scatter between Eq. (1) and FE

results on interval $[0, \pi]$. The coefficients $\lambda_i/\sigma_{\text{nom}}$ are reported in Figure 2. Obviously, other choices to evaluate the coefficients λ_i are possible, for example, by imposing the exact agreement in three points between σ_θ and $\sigma_{\theta,FE}$. In the case of figure 2, the $e\%$ is 3.9% in the interval $[0, \pi]$.

In order to check Eqs (6–8), an experimental investigation could be made by means of resistance strain gauges as will be shown in a next section. If the thickness of the plate is sufficiently large, the strain gauge can be positioned on the free border with the axis exactly on the middle plane. Then, the trend of the hoop stress σ_θ can be calculated directly through the measured strain by imposing a plane strain or plane stress condition. On the other hand, if the thickness is only a few millimetres or the hole is not large enough with respect to the grid of the strain gauge a direct measurement on the free border of the hoop strain is not possible. So that an alternative way should be used. Accurate FE analysis has shown that the first invariant stress tensor I_θ has a hyperbolic trend near the hole border also far from the former case proposed by Kirsh [23]. On the basis of this observation, we assume that the trend of I_θ will be hyperbolic in the form:

$$I_\theta = A + \frac{B}{r^2} \quad (9)$$

A and B being two parameters that depend on the boundary condition. If one knows the value of I_θ at two different locations, A and B can be easily evaluated and then also the stress at the free border because σ_θ agrees with I_θ under plane stress conditions.

Figure 3 shows a comparison between the hoop stress calculated directly on the free border and that has been extrapolated with equation (9). The agreement is very satisfactory. Furthermore, from Figure 3, the trend of I_θ as a function of η angle can be expressed as the sum of dimensionless stress function Eqs (6–8) previous assessments of λ_i coefficients.

3. Stress Intensity factor assessments

Keeping in mind the stress intensity factors of cracks in flat plates, the crack can be replaced with an equivalent ellipse. If we relate the maximum hoop stress to the SIF as in Refs [10, 14], the tip notch radius has to be very small compared with the crack length. The new approach based on the J-integral could be used to obtain high accuracy with a tip notch radius that is not small enough [20]. As a latter simplification, the ellipse can be replaced by a circular hole as

reported in Figure 4. The high accuracy obtained in Ref. [20] in the use of the J-integral is due to the particular decomposition of the hoop stress on the free edge of the equivalent ellipse given by Eqs (2–4). The relationship between the J-integral of the crack in point A of Figure 4a and the J-integral of the equivalent notch (namely $J_{V\rho}$) in point A' of Figure 4b, is considered without taking into account the terms that give a secondary contribution when the ellipse becomes a crack. Therefore, in this way, the errors are around a few percent but the advantage is that there is no longer the problem of stress singularity due to the presence of the crack in the FE model or in an experimental analysis. Furthermore, in this paper, the idea is to substitute the crack with an equivalent circular hole in order to allow us to simplify the experimental assessment of the SIF by means of the strain gauge technique and extend the idea to a sheaf of straight cracks around the centre of the equivalent hole.

The dimensionless stress component (6–8) can be used for the assessment of $J_{V\rho}$ along an integration path Γ between the two points from A' to B' as showed in Figure 4.

In terms of computational efficiency, it is positively helpful to assess the $J_{V\rho}$ between the two points B' and C' by taking into account the hoop stress along the free surface [16,18]. For a linear elastic material we have:

$$J_{V\rho} = \int_{-\frac{\pi}{2}}^{\frac{\pi}{2}} \frac{\rho \sigma_{\theta}^2}{2E'} \cos(\theta) d\theta \quad (10)$$

where E' represents the elastic modulus E of the material under plane stress conditions and E' is equal to $E / (1 - \nu^2)$ under plane strain conditions (ν Poisson's ratio).

Since $J_{V\rho}$ is calculated on the free surface of the notch, it is linked only to three stress terms: $\sigma_{\theta,1}^2$, $\sigma_{\theta,2}^2$, $\sigma_{\theta,3}^2$ and $2 \cdot \sigma_{\theta,1} \cdot \sigma_{\theta,3}$. Note that the others terms are null because the odds of the functions under the integral sign. From Eqs (6–8), the $J_{V\rho}$, related to the stress components $\sigma_{\theta,i}$ is:

$$J_{V\rho} = \sum_{i=1}^4 J_{V\rho,i} \quad (11)$$

$$J_{V\rho,1} = \int_{-\frac{\pi}{2}}^{\frac{\pi}{2}} \frac{\rho \lambda_1^2 \sigma_{\theta,1}^2}{2E'} \cos \theta d\theta = \frac{7}{15} \frac{\rho \lambda_1^2}{E'} \quad (12)$$

$$J_{V\rho,2} = \int_{-\frac{\pi}{2}}^{\frac{\pi}{2}} \frac{\rho \lambda_2^2 \sigma_{\theta,2}^2}{2E'} \cos \theta d\theta = \frac{8}{15} \frac{\rho \lambda_2^2}{E'} \quad (13)$$

$$J_{V\rho,3} = \int_{-\frac{\pi}{2}}^{\frac{\pi}{2}} \frac{\rho \lambda_3^2 \sigma_{\theta,3}^2}{2E'} \cos \theta d\theta = \frac{23}{15} \frac{\rho \lambda_3^2}{E'} \quad (14)$$

$$J_{V\rho,4} = \int_{-\frac{\pi}{2}}^{\frac{\pi}{2}} \frac{2\rho \lambda_1 \lambda_3 \sigma_{\theta,1} \sigma_{\theta,3}}{2E'} \cos \theta d\theta = \frac{26}{45} \frac{\rho \lambda_1 \lambda_3}{E'} \quad (15)$$

From Eqs (12–15), the $J_{V\rho}$ is known as soon as the coefficients λ_i are calculated from FE analysis or by means of an experimental analysis of equivalent model of Figure 4b where the crack is replaced with an hole.

As underlined in [20], on the basis of many accurate FE analyses, when the equivalent notch becomes a crack, Eqs (14) and (15) do not give any contributions to $J_{V\rho}$. In others words, only Eqs (12) and (13) are directly related to the J-integral of the initial crack model. For this reason, we consider $J_{V\rho,3}$ and $J_{V\rho,4}$ as spurious values. This is a fundamental question because when we substitute the crack with a hole, the weight of the two spurious terms $J_{V\rho,3}$ and $J_{V\rho,4}$ could have the same size as the others two fundamental contributions $J_{V\rho,1}$ and $J_{V\rho,2}$ [20].

Now we are able to evaluate the SIF of the initial crack from a comparison between the classical J-integral on path Γ of Figure 4a and the $J_{V\rho}$ on path Γ' of Figure 4b. The relation between the classical J-integral and $J_{V\rho}$ is given by the following relation [12]:

$$J_I = \frac{K_I^2}{E'} = \frac{5\pi}{21} J_{V\rho,1} \quad (16)$$

for mode I loading, and

$$J_{II} = \frac{K_{II}^2}{E'} = \frac{15\pi}{128} J_{V\rho,2} \quad (17)$$

for mode II loadings.

Finally, in virtue of Eqs (12–13) and Eqs (16–17) the K_I and K_{II} of the crack in point A of Figure 4a is given in this form

$$K_I^2 = \frac{\pi \rho \lambda_1^2}{9 E'} \quad (18)$$

$$K_{II}^2 = \frac{\pi \rho \lambda_2^2}{16 E'} \quad (19)$$

From an operative point of view, after the stress analysis of the equivalent model of Figure 4b, we first evaluate the λ_i coefficients and then, by means of Eqs (18, 19) the K_i can be easily estimated. The stress analysis can be performed or by the direct evaluation of the hoop stress σ_θ on the free border of the bore or, alternatively, by means of the extrapolation technique addressed by Eq. (19).

Now, if we rotate the crack of a β angle as in Figure 5, the SIF can be rapidly evaluated by observing that the λ_i coefficients should be calculated without making a new stress analysis, because if we rotate the crack of a β angle, the hoop stress in a rotated (x', y') coordinate system can be expressed as a function of hoop stress in the (x, y) coordinate system as: $\sigma_\theta(\eta) = \sigma_\theta(\eta' + \beta)$. In other words, with a single stress analysis made in a (x, y) coordinate system, it is possible to evaluate all SIF of the sheaf of straight cracks around the centre of the equivalent hole by simply rotating the stress field on the free border. For example, in Figure 6.a the actual crack between two holes subjected to a uniform remote stress is replaced by a hole in Figure 6.b. By means of single FE analysis the SIF of mode I and II is evaluated in Table 1 with Eqs (18) and (19) for many β angle. Table 1 shows a comparison among different methods in the SIF assessment: 1) expansions of complex stress potentials referred to an infinite plate given by Newman (see Tada et al. [24]); 2) asymptotic FE analysis with very fine mesh by performing the K_i with a linear regression in double logarithmic scale of the hoop stress along the bisector as indicated in Ref. [25]; 3) Eqs (16–17). The difference between asymptotic FE analysis and the method of equivalent hole is around 2–3%.

4. Experimental analysis of plates under mixed mode loadings

In order to confirm the prediction on hoop stress distribution on the free border (Eqs 6–8) and in proximity of a circular hole (Eq. 9) two plates under mixed mode loadings (model I plus mode II) have been analysed. Figure 7 shows two plates made of aluminium alloy with two different bore diameters. The first plate of Figure 7.a has a bore with a diameter equal to a half width plate whereas the plate of Figure 7.b has a bore with a diameter equal to a fifth of the width. In the first case, it is possible to locate 12 strain gauges on the middle plane along the free border with the grid axis parallel to the tangential direction (see Figure 8a). For the second plate, only three strain gauges were located on the free border because the bore has a minor diameter (strain gauge 17, 18 and 19). The other strain gauges were located on the free surface with a tangential step of 45° on two different circumferences with a nominal distance from the free border of 3 and 10 mm, respectively. Furthermore, a phase angle of 22.5° was considered between the strain gauges on the two circumferences. The strain gauges (1, 3, 6, 8, 10, 11, 13 and 16) had the grid axis along the radial direction, strain gauges (2, 4, 5, 7, 9, 12, 14 and 15) had the grid axis along the tangential direction. By summing the strain of two opposite strain gauges respect the centre of the bore, we obtain the first invariant of the strain tensor. Then, by means of the linear elastic relations, the first invariant of the stress tensor I_θ can be calculated. In this way, we have four measurements of I_θ at a nominal distance of 3 mm (2.8 average actual distance) and four measurements of I_θ at a nominal distance of 10 mm (9.8 average actual distance) from the free border.

The device of Figure 9 was used to subject the plates of Figure 7 to mixed mode loading. By setting a couple of external holes, the local load condition changed from pure mode I loading to main mode II loading.

In all experimental cases, the load was applied from zero to a maximum value of about 6kN in many steps. Then, the experimental measurements given by the strain gauges were statistically analysed and a linear regression was used in order to calculate the reference value for a load of 30 kN. Figure 10 reports a typical trend of measured strains on the surface for the plate of Figure 7b.

All the analyses are calculated by imposing a to plane stress loading conditions on all points of the plate. In fact the ratio between the thickness and the curvature radius assures a wide plane stress condition along the free border [26, 27].

4.1 Hoop stress calculation on the free border with strain gauges attached to the mid plane.

Figure 11 shows the results of a whole series of experimental measurements performed from the 12 strain gauges attached to the free border of the bore with a diameter equal to 50 mm. The stresses are reported in dimensionless form for load angles ψ of 0, 45 and 90 degrees, respectively (similar results for others load directions have been obtained). Figure 12, instead, shows the results obtained for the plate with the bore diameter of 20 mm. In this case, the strain gauges are only 3. The load ψ angle is the same as Figure 11. In both cases, the results can be considered satisfactory. Equation (1) is able to describe the trend of the hoop stress along the free border also for the case of the bore of 50 mm where the condition of the isolated hole is no longer respected.

4.2 Hoop stress on the free border with strain gauges attached to the surface of the plate

When the thickness of the plate is thin compared to the size of the strain gauge, we can use the strain gauge configuration of Figure 7b for the evaluation of the hoop stress on the free border. By summing the two opposite strain gauge signals with respect to the centre of the bore we obtain the first strain invariant, thus, by means of the linear elastic relations I_{θ} can be calculated. Figure 13 shows the trend of the first stress invariant I_{θ} at distance $r=3$ mm from the free border for two directions of the force: $\psi=0^{\circ}$ and $\psi=45^{\circ}$. The four values of I_{θ} given by the strain gauges, are interpolated by means of dimensionless stress function (6-8) obtaining Eq. (1) from the trend of I_{θ} all around the bore (dash lines). Finally, a comparison with the FE prediction of I_{θ} is made (solid lines).

Now, we can also evaluate the first stress invariant I_{θ} at distance $r=10$ mm from the free border and by taking advantage of Eq. (9), the trend of σ_{θ} at the free border is evaluated. Figure 14, proposes the extrapolated values of I_{θ} and the stress prediction with the three strain gauges 17–18-19 attached to the border.

4.3 SIF assessment from strain gauge measurements on an equivalent hole

On the basis of the stress analysis on the free border as proposed above, the SIF of a crack can be estimated for a crack of a length equal to the bore diameter. In order to check the accuracy of Eqs 18–19, table 2 reports a comparison between the analytical prediction and FE results. When the crack was simulated in the FE model, a very fine mesh was used with elements of size about 10^{-4} mm at the notch tip and the SIFs were calculated with a regression as described in Ref. [25]. The analytical predictions with Eqs 18–19 are based on the analysis of the hoop stress calculated with FE results by substituting the crack with an equivalent hole. From the FE results, the λ_i coefficients were calculated by imposing a minimum scatter between Eq. (1) and the FE results. The mode I stress intensity factor is calculated with an errors less than 10% also with a bore diameter equal to 50% of the width. On the contrary, the mode II stress intensity factor needs a small diameter to achieve good accuracy.

The results of the experimental measurements on the plate of Figure 7b are reported in table 3. The SIFs obtained by simulating the crack in a FE model are compared with the results given by Eqs (18 and 19) where the stress analysis at the equivalent hole was performed in a different way: 1) Equivalent hole with FE stress analysis on the free border; 2) Equivalent hole with strain gauges on the free border, 3) Equivalent hole with a strain gauges on the surface. The crack has a tilt angle θ equal to 30° , whereas the load direction ψ is equal to 0 and 90 degree, respectively.

The experimental average error in the mode I SIF prediction is around the maximum error obtained with FE results by using the equivalent hole method. However, for mode II loading the experimental average error is higher than the FE prediction and may be due to experimental noise such as the out of plane bending measured by the couple of strain gauges (attached to the two surfaces) far from the bore along the longitudinal axis (see Figure 8b). This issue will be explored further in the future.

5. CONCLUSIONS

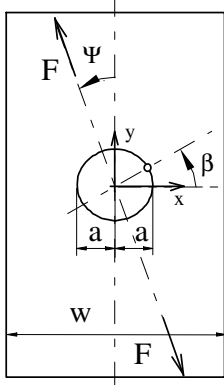
This paper has highlighted, from the experimental and numerical point of view, that the hoop stress on the free edge of a hole can be useful to calculate the stress intensity factors (SIF) of cracks with a size equal to the bore diameter. The main conclusion can be summarised as follows:

- By replacing the crack with an equivalent hole, based on finite element analysis or strain gauge experimental investigations, it was possible to derive the values of the SIF of the sheaf of straight cracks around the centre of the equivalent circle.
- The average experimental error is lower than 10% for the mode I. For the mode II, there was greater sensitivity of the experimental SIF to experimental noise.
- The technique of the equivalent hole is applicable to both thick plates (strain gauges attached on the thickness) and thin plates (strain gauges attached on the surface near the hole free border).

Table 1: Prediction of shape factor Y by means of an equivalent hole for the crack of Figure 6a.

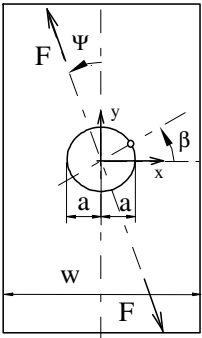
SIF points A $Y_i = \frac{K_i}{\sigma_{nom} \sqrt{\pi a}}$	FE analysis by modelling the crack		Equivalent hole Eqs (18–19) with FE hoop stress on the free border		Newman 1971 [24]
	Y _I	Y _{II}	Y _I	Y _{II}	Y _I
$\theta=0^\circ$	0.727	0.001	0.730	0.000	0.730
$\theta=30^\circ$	0.547	0.285	0.588	0.299	-
$\theta=60^\circ$	0.204	0.276	0.212	0.299	-
$\theta=90^\circ$	0.043	0.000	0.039	0.000	-

Table 2: Stress Intensity Factors obtained point A for different crack sizes by means of the equivalent hole. The plate is similar to that of Figure 7.a loaded with the device of Figure 9: $\psi=60^\circ$, $\beta=0^\circ$ ($F=30$ kN, $w=100$ mm, hoop stress from FE analysis).



a [mm]	$2a/w$	$K_{I,Jv\rho}$ [MPa mm ^{0.5}]	$K_{I,FE}$ [MPa mm ^{0.5}]	$\frac{K_{I,Jv\rho}}{K_{I,FE}}$ [%]	$K_{II,Jv\rho}$ [MPa mm ^{0.5}]	$ K_{II,FE} $ [MPa mm ^{0.5}]	$\frac{K_{II,Jv\rho}}{ K_{II,FE} }$ [%]
25	0.5	293	272	8	977	611	59
15	0.3	198	191	4	539	453	19
10	0.2	155	152	2	396	366	8

Table 3: Stress intensity factors in point A obtained with different methods. Plate of Figure 7b loaded by means of the device of Figure 9 ($F=30$ kN, $\beta=30^\circ$, $a=10$ mm, $w=100$ mm on the bracket the percent errors respect the asymptotic FE analysis).

	FE analysis by modelling the crack		Equivalent hole with FE stress on the free border		Equivalent hole with strain gauge on the free border		Equivalent hole with strain gauge on the surface	
	$K_{I,FE}$	$K_{II,FE}$	$K_{I,FE}$	$K_{II,FE}$	$K_{I,Jvp}$	$K_{II,Jvp}$	$K_{I,Jvp}$	$K_{II,Jvp}$
	[MPa mm ^{0.5}]	[MPa mm ^{0.5}]	[MPa mm ^{0.5}]	[MPa mm ^{0.5}]	[MPa mm ^{0.5}]	[MPa mm ^{0.5}]	[MPa mm ^{0.5}]	[MPa mm ^{0.5}]
$\psi = 0^\circ$	216	122	216 (0%)	129 (5.7%)	216 (0%)	144 (18%)	198 (8.3%)	122 (11%)
$\psi = 45^\circ$	416	60.8	436 (4.8%)	63 (3.6%)	454 (9.1%)	48 (21%)	416 (0%)	45 (26%)

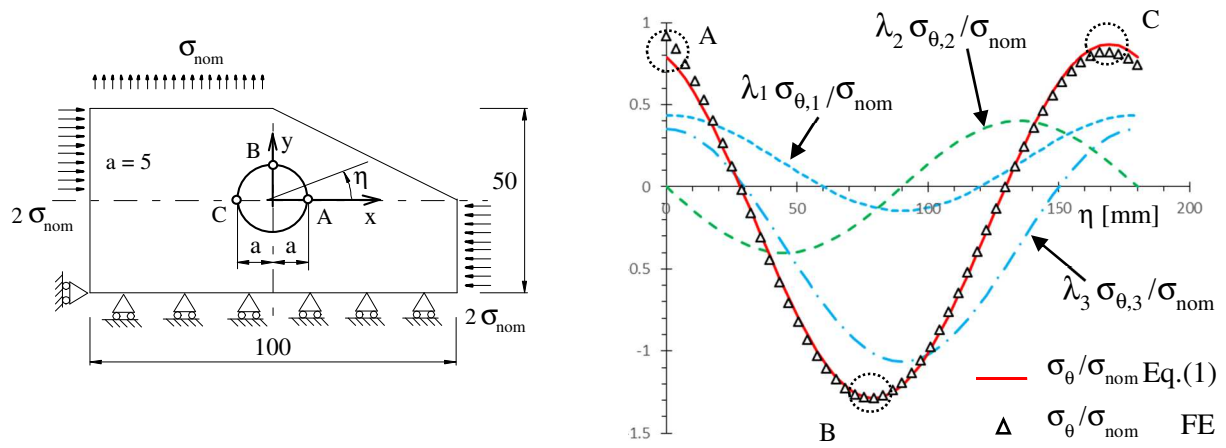


Figure 2: Hoop stress along the free border of the hole obtained as a sum of the three dimensionless stress $\sigma_{\theta,i}$ (dimensions in millimetres, $\lambda_1/\sigma_{nom}= 0.437$, $\lambda_2/\sigma_{nom}= -0.401$, $\lambda_3/\sigma_{nom}= 0.355$)

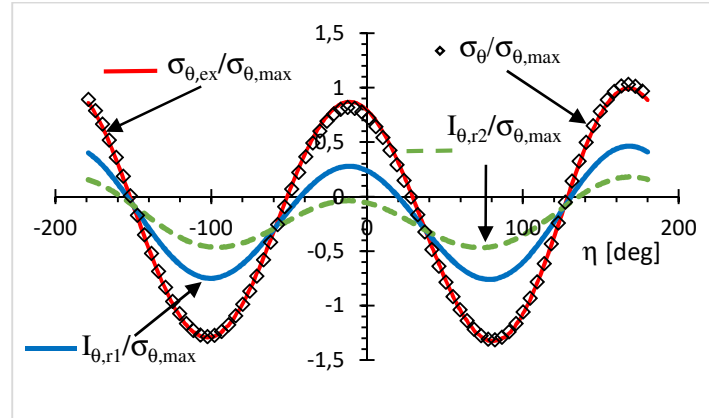
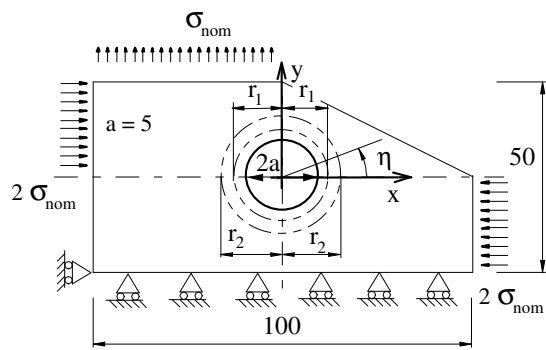


Figure 3: Dimensionless stresses with respect to the maximum hoop stress $\sigma_{\theta,\max}$ at the free border of the hole. Results from FE analysis ($\sigma_{\theta,\text{ex}}$ = extrapolated hoop stress from first invariant stress tensor $I_{\theta,r1}$ and $I_{\theta,r2}$ by means of Eq. (9), dimensions in millimetres, $a=5$ mm, $r_1=7$ mm, $r_2=10$ mm)

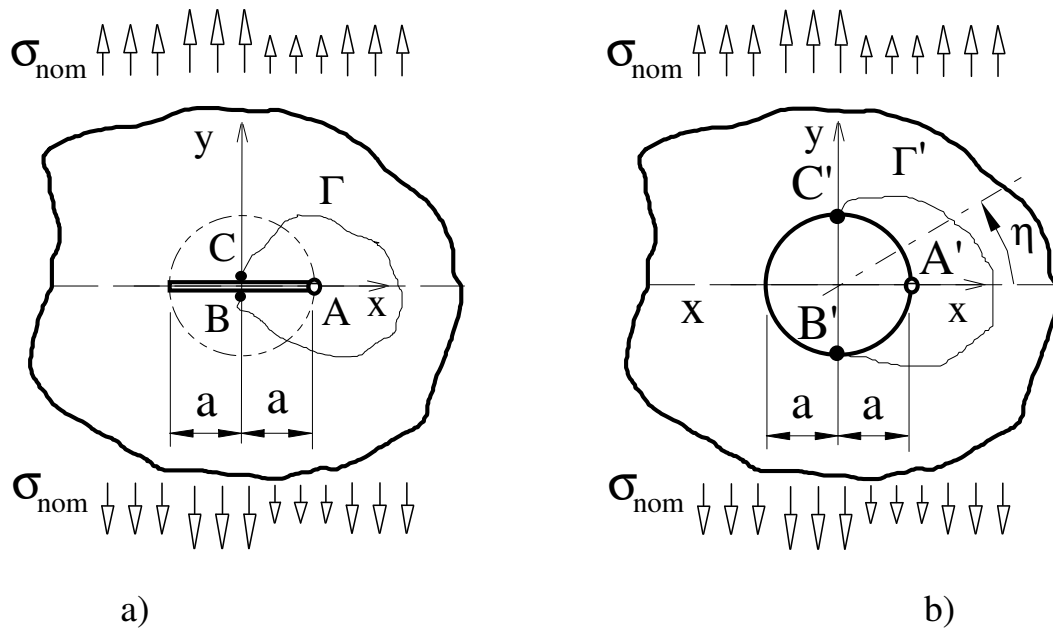


Figure 4: Actual geometry with the crack (a) and plate with the equivalent hole (b) used for FE analysis (paths Γ and Γ' are related to the assessments of SIF at point A)

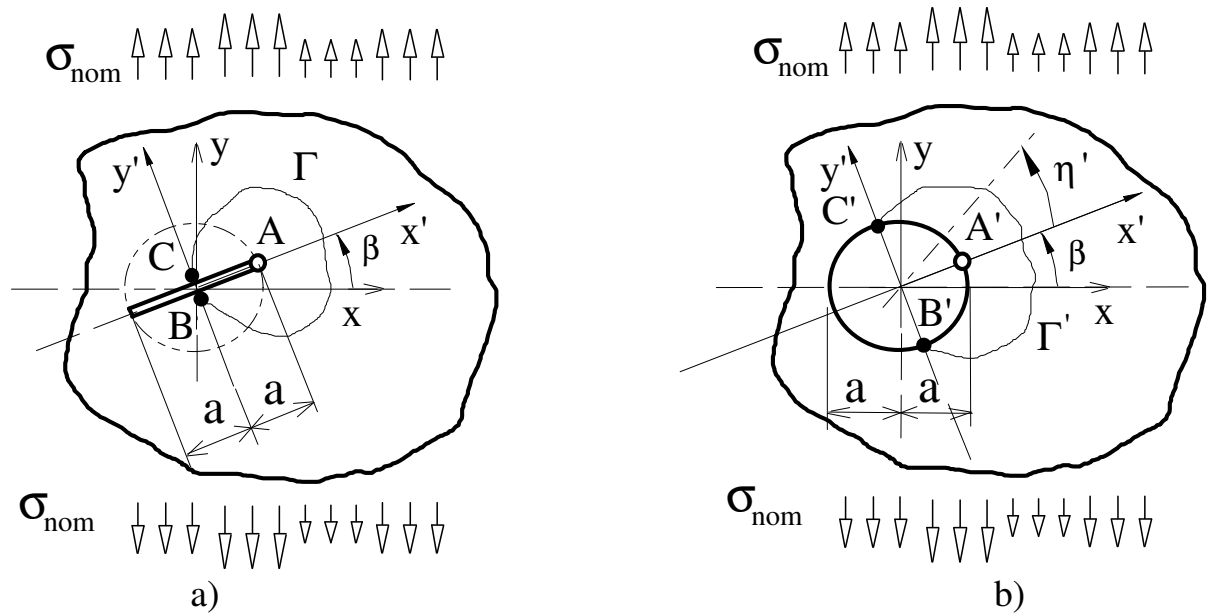


Figure 5: Actual geometry with a rotate crack (a) and plate with the equivalent hole (b) used for FE analysis (paths Γ and Γ' are related to the assessments of SIF at point A)

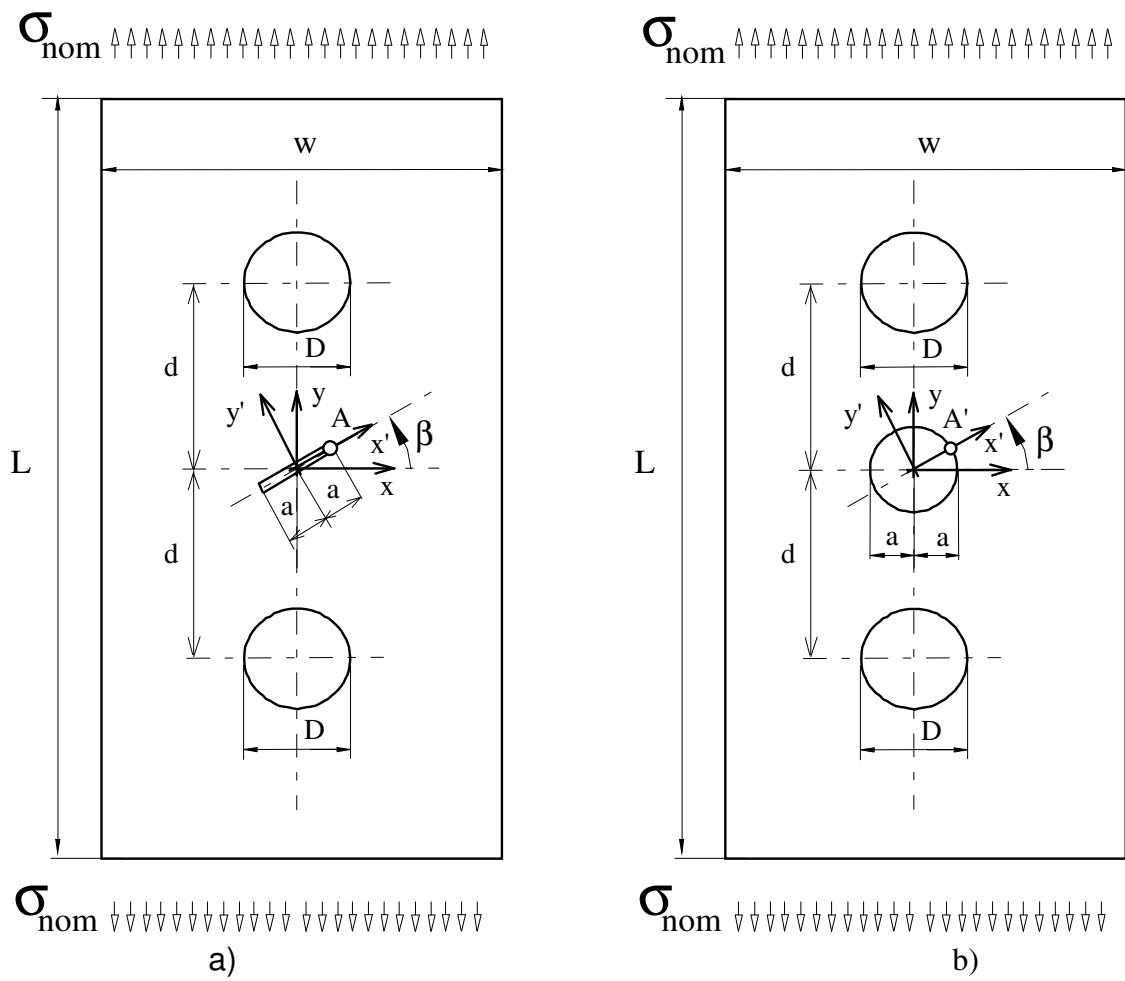


Figure 6: Crack near two holes under tensile loading ($a=5$ mm, $w/a=80$, $L/a=320$, $D/a=4$, $d/a=8$).

- a) Actual geometry with the crack rotated at β angle
- b) Equivalent hole model for FE analysis

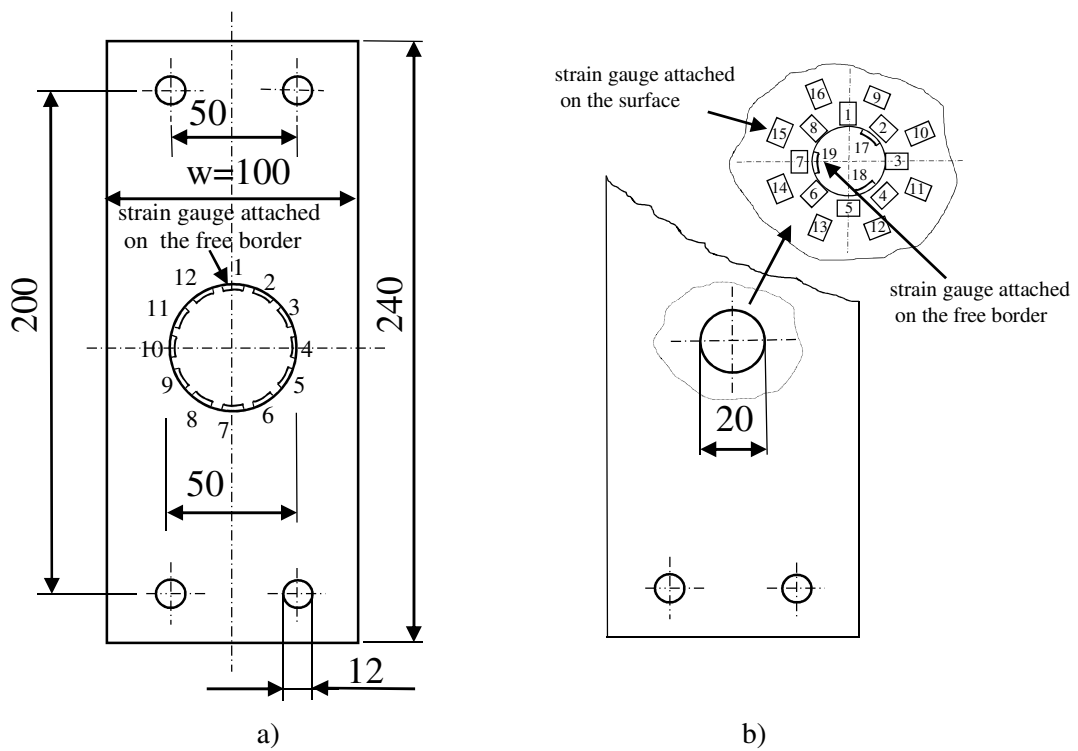
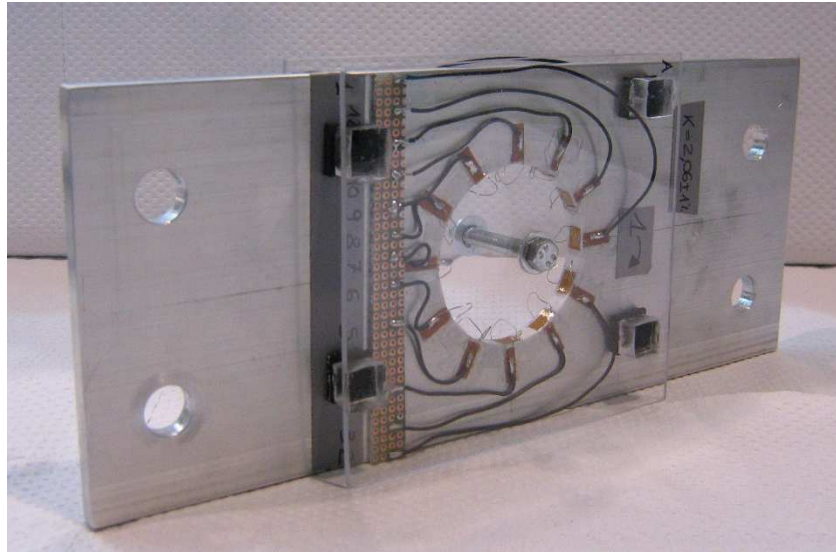
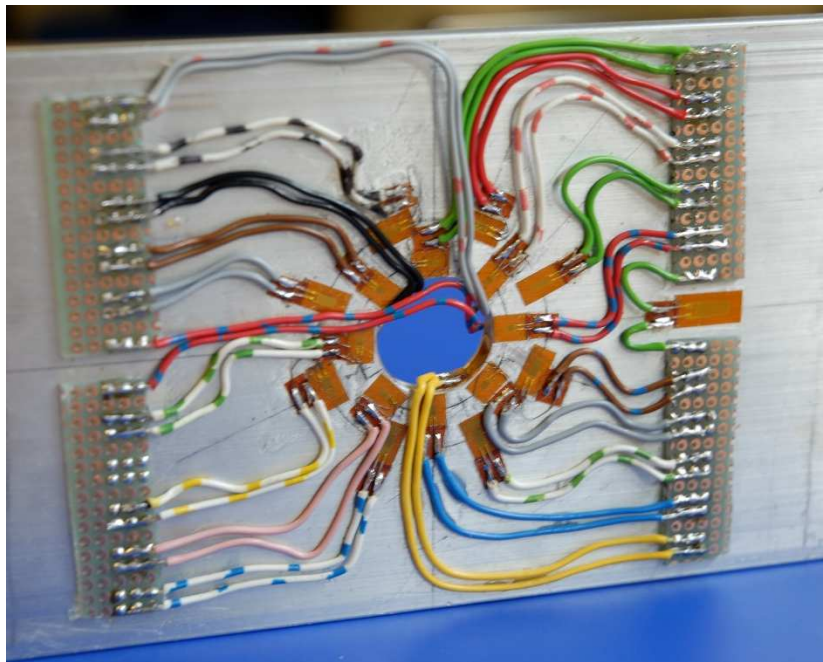


Figure 7: Dimension of an aluminium alloy plate with strain gauge (thickness 6 mm, $E=70600$ MPa, $\nu=0.33$)

- a) Plate with a bore diameter of 50 mm (diameter/ $w=0.5$)
- b) Plate with a bore diameter of 20 mm (diameter/ $w =0.2$)



a)



b)

Figure 8: Photos of an aluminium alloy plate with strain gauge
a) Plate with a bore of 50 mm with strain gauge on the border
b) Plate with a bore of 20 mm with strain gauge on the border and on the surface of the plate

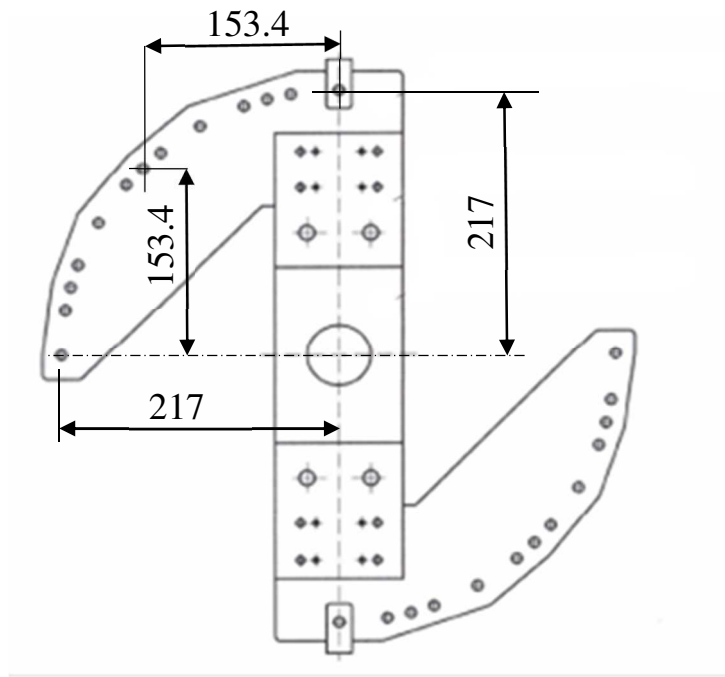


Figure 9: Device for mixed mode loading

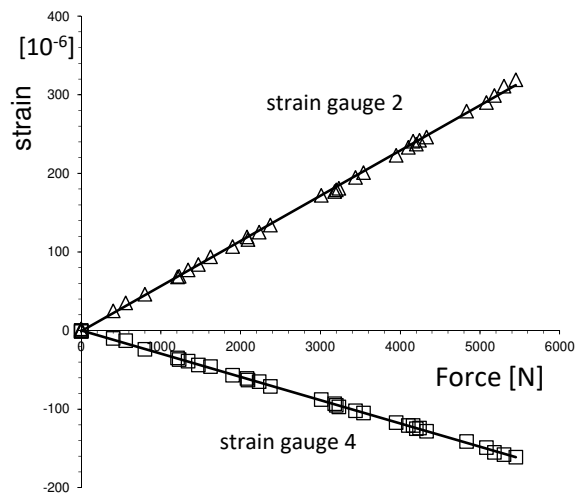


Figure 10: Typical strain measurement of strain gauges 2 and 4 for the plate of Figure 7b for $\psi=45^\circ$

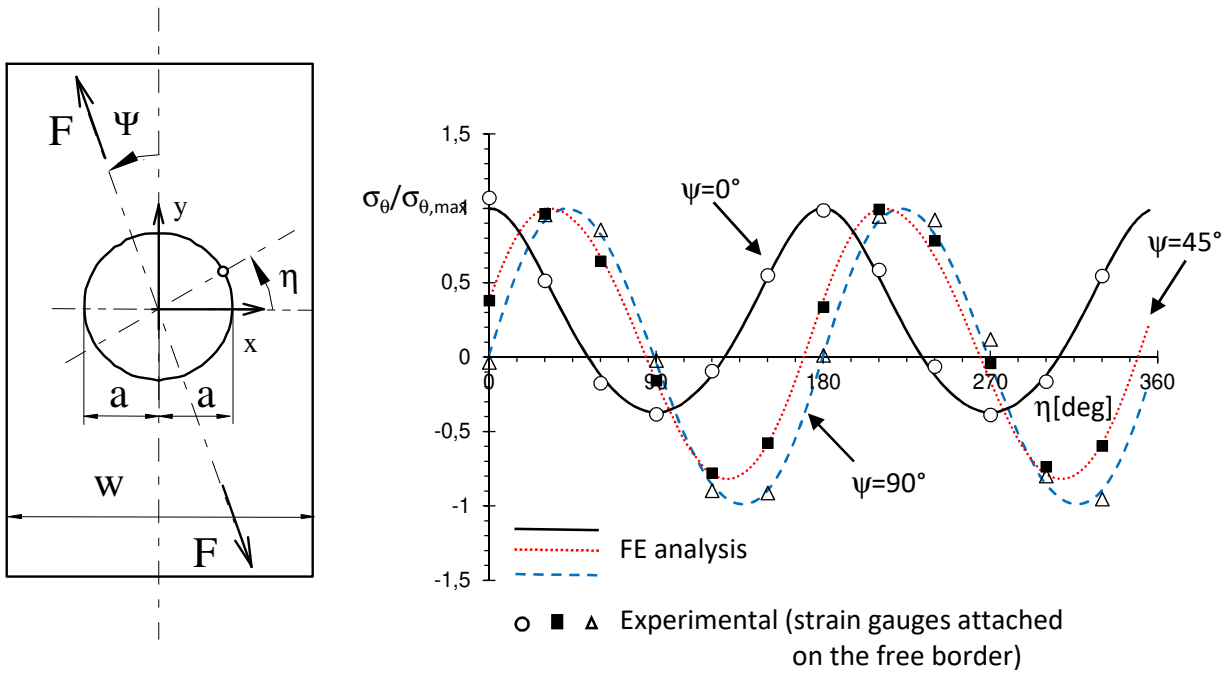


Figure 11: Hoop stress on the free border evaluated by means of strain gauges of Figure 7a. Dimensionless value with respect to the maximum FE hoop stress $\sigma_{\theta, \max}$ ($a=25$ mm, $2a/w=0.5$)

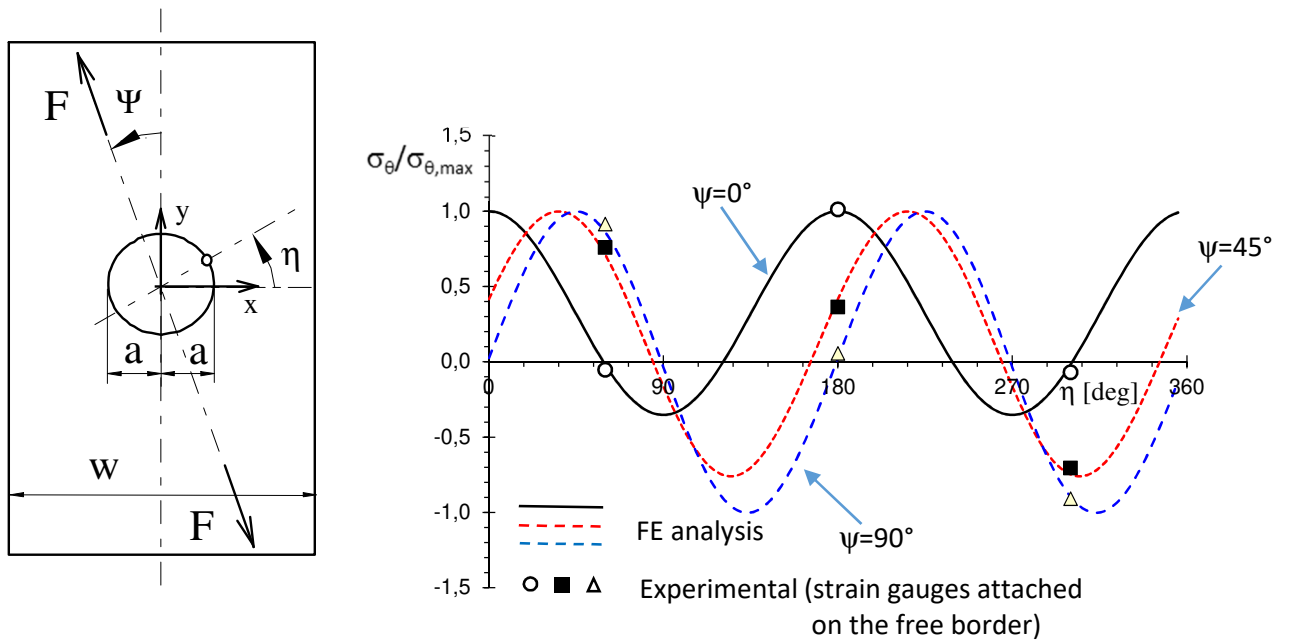


Figure 12: Hoop stress on the free border evaluated by means of strain gauges of Figure 7b. Dimensionless value with respect to the maximum FE hoop stress $\sigma_{\theta, \max}$ ($a=10$ mm, $2a/w=0.2$; w is the plate width)

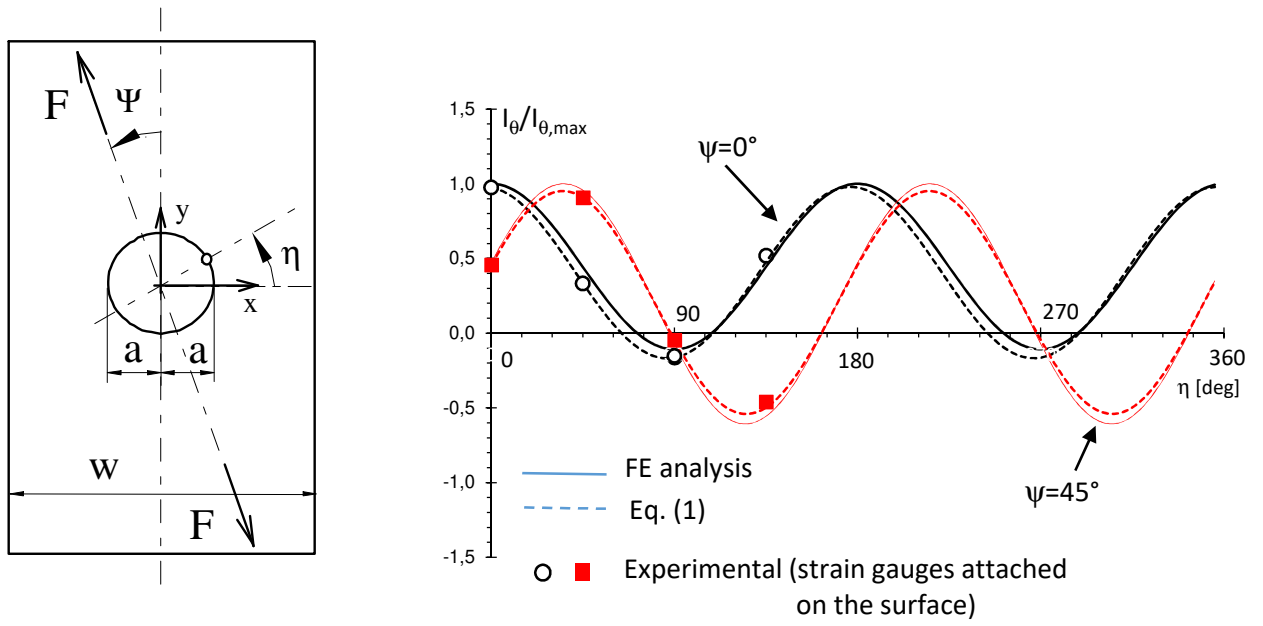


Figure 13: First invariant stress tensor I_θ evaluated by means of strain gauges of Figure 7b at a distance of 3 mm from the border. Dimensionless values with respect to the maximum FE hoop stress $\sigma_{\theta, \max}$ ($a=10$ mm, $2a/w=0.2$)

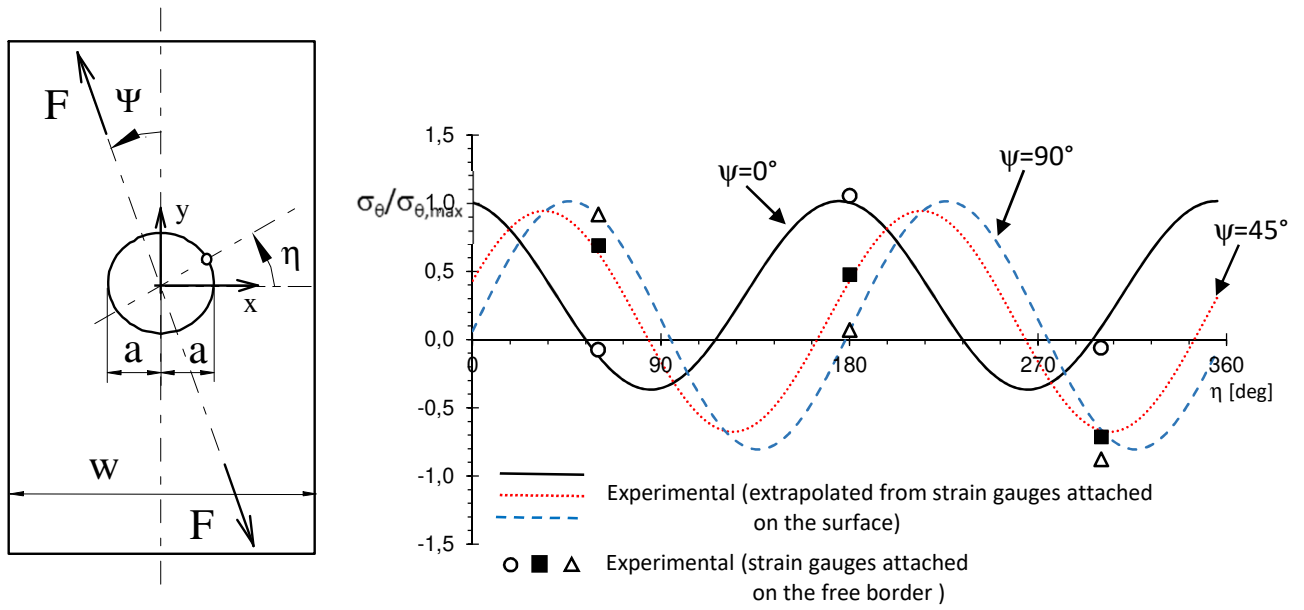


Figure 14: Hoop stress on the free border of Figure 7b extrapolated from the first invariant stress tensor I_θ evaluated with Eq. (9) by means of strain gauges at a distance of 3 and 10 mm, from the free border, respectively. Dimensionless value with respect to the maximum FE hoop stress $\sigma_{\theta, \max}$ ($a=10$ mm, $2a/w=0.2$)

-
- ¹ Tomlinson R.A., Nurse A.D., Patterson E.A. *Fatigue Fract. Engng Mater Struct.*, 20 (2), pp 217–226, 1997
- ² A. Kotousov, Z. He, A. Fanciulli, Application of digital image correlation technique for investigation of the displacement and strain fields within a sharp notch, *Theoretical and Applied Fracture Mechanics* 79, 2015, 51–57
- ³ Picon R., Paris F., Canas J., Marin J. A complete field method for the photoelastic determination of K_I and K_{II} in general mixed-mode fracture *Engng Fract. Mech.* 51, 505–516, 1996
- ⁴ Radaj D, Local fatigue-strength characteristic values for spot-welded joints, *Engng Fract Mech.* 1990, 37 (1), 245–250
- ⁵ S.-P. Chiew, C.-K. Lee, S.-T. Lie, H. Li Ji, Fatigue behaviors of square-to-square hollow section, *Engineering Fracture Mechanics* 74, 2007, 703–720
- T-joint with corner crack. I: Experimental studies
- ⁶ Partanen T. and Niemi E., Hot spot stress approach to fatigue strength analysis of welded components: fatigue test data for steel plate thicknesses up to 10 mm, *Fatigue Fract. Engng Mater. Struct.* 19, 6, pp 709–722, 1996
- ⁷ Niemi E., Fricke W. and Maddox S.J., Fatigue analysis of welded components, designer guide to the structural hot spot weld stress approach, II W, 1430–00, 2006
- ⁸ Lazzarin P., Tovo R. A notch stress intensity factor approach to the stress analysis of welds. *Fatigue & Fracture of Engineering Materials and Structures* 1998:21:1089–1103
- ⁹ Williams M.L.. Stress singularities resulting from various boundary conditions in angular corners of plates in extension. *Journal of Applied Mechanics* 1952, 19, 526–528
- ¹⁰ Irwin G.R., *Fracture In Hanbuck der physik, VI, Elasticity and Plasticity*, 551–590, Springer-Verlag, Berlin, 1958
- ¹¹ Neuber H., *Theory of Notch Stresses: principles for exact calculation of strength with reference to structural form and material*, Second Enlarged Edition, Springer-Verlag, Berlin, 1958
- ¹² Livieri P., Segala F., Analytical evaluation of J-integral for elliptical and parabolic notches under mode I and mode II loading, *International Journal of Fracture*, 148, 57–7, 2007

-
- ¹³ Shin C.S., Man K.C., Wang C.M., A practical method to estimate the stress concentration of notches. *International Journal of Fatigue*, 16, 242–256, 1994
- ¹⁴ Sih G.C., Liebowitz H., Mathematical theories of brittle fracture. In *Fracture: an advanced treatise*, edited by Liebowitz H., Vol. II Mathematical Fundamentals, 1968, pp 67–190
- ¹⁵ Aliabadi M.H., Rooke D.P.. *Numerical Fracture Mechanics*, Kluwer Academic Publishers 1991
- ¹⁶ Rice J.R., A path independent integral and the approximate analysis of strain concentration by notches and cracks. *ASME-Journal of Applied Mechanics*, **35**, 379–386, 1968
- ¹⁷ Livieri P., Segala F., Analytical evaluation of J-integral for elliptical and parabolic notches under mode I and mode II loading, *International Journal of Fracture*, 148, 57–7, 2007
- ¹⁸ P. Livieri P., A new path independent integral applied to notched components under mode I loadings. *International Journal of Fracture*, 123, 107–125, 2003
- ¹⁹ P. Livieri P., Use of J-integral to predict static failures in sharp V-notches and rounded U-notches. *Eng Fract Mech.* 2008, 75:1779–1793
- ²⁰ P. Livieri P., Segala F., An analysis of three-dimensional planar embedded cracks subjected to uniform tensile stress, *Engineering Fracture Mechanics*, Volume 77, 2010, pp 1656–1664
- ²¹ Inglis C.E., Stresses in a plate due to the presence of cracks and sharp corners. *Transactions Institution of Naval Architects* 55, 219–230, 1913
- ²² Zappalorto M., Lazzarin P., Three-dimensional elastic stress fields ahead of notches in thick plates under various loading conditions, *Engineering Fracture Mechanics* 108 (2013) 75–88
- ²³ Kirsch G.,: *Die Theorie der Elastizitat and die Bediirfnisse der Festigkeitslehre.* Z. Vereines Deutscher Ing. 1898, 42, 797–807
- ²⁴ Tada H., Paris C.P., Irwin G.R., *The stress analysis of cracks handbook.* Third edition, ASME, New York. 2000
- ²⁵ Lazzarin P., Livieri P. Notch Stress Intensity Factors and fatigue strength of aluminium and steel welded joints, *International Journal of Fatigue*, 23 (3), 2001, pp 225–232
- ²⁶ Livieri P., Nicoletto G. Elasto-Plastic Strain Concentration Factors in Finite Thickness Plates, *The Journal of Strain Analysis for Engineering Design*, January 2003, Volume 38 Issue 1, pp 31–36
- ²⁷ F. Berto and C. Marangon, Three-dimensional effects in finite thickness plates weakened by rounded notches and holes under in-plane shear, *Fatigue & Fracture of Engineering Materials and Structures*, 2013, 36 (11) Pages 1091–1208
